Pathogenesis of Experimental Ebola Virus Infection in Guinea Pigs

Brett M. Connolly, Keith E. Steele, Kelly J. Davis, Thomas W. Geisbert, Wayne M. Kell, Nancy K. Jaax, and Peter B. Jahrling

Virology and Pathology Divisions and Headquarters, United States Army Medical Research Institute of Infectious Diseases, Fort Detrick, Frederick, Maryland

The subtype Zaire of Ebola (EBO) virus (Mayinga strain) was adapted to produce lethal infections in guinea pigs. In many ways, the disease was similar to EBO infections in nonhuman primates and humans. The guinea pig model was used to investigate the pathologic events in EBO infection that lead to death. Analytical methods included immunohistochemistry, in situ hybridization, and electron microscopy. Cells of the mononuclear phagocyte system, primarily macrophages, were identified as the early and sustained targets of EBO virus. During later stages of infection, interstitial fibroblasts in various tissues were infected, and there was evidence of endothelial cell infection and fibrin deposition. The distribution of lesions, hematologic profiles, and increases in serum biochemical enzymes associated with EBO virus infection in guinea pigs was similar to reported findings in experimentally infected nonhuman primates and naturally infected humans.

The recent reemergence of Ebola (EBO) virus in highly fatal outbreaks occurring in the Democratic Republic of the Congo (DRC) and Gabon has focused international attention on this deadly pathogen. EBO and Marburg viruses form the family Filoviridae and are responsible for devastating, lethal hemorrhagic fevers in human and nonhuman primates [1–11]. Historically, filovirus outbreaks have been isolated and sporadic, suggesting that these viruses persist in nature until undefined environmental changes (natural or human made), ecologic conditions, or demographic factors enable them to resurface. Despite intensive epidemiologic research, the natural host of filoviruses has yet to be identified.

Two serologically distinct subtypes of EBO virus (Zaire [EBO-Z] and Sudan) were first identified in 1976 after two major simultaneous epidemics that centered in Yambuku, DRC, and Maridi, Sudan [6, 7, 12–14]. In 1989, the discovery of a third strain of EBO virus, subtype Reston (EBO-R) in an animal facility in the United States alarmed the biomedical community [15]. EBO-R has since been isolated from several other monkey shipments originating from the Philippines [16–19]. Although there is serologic evidence of human infection with EBO-R, no deaths have resulted [20, 21]. A genetically distinct fourth strain of EBO, which is lethal for some monkey species and has unknown pathogenicity in humans, was isolated from a nonfatal human case in Côte d'Ivoire [22].

In sharp contrast, during the well-publicized 1995 outbreak of EBO hemorrhagic fever in and around Kikwit, DRC, there were 245 deaths (77% mortality) [23, 24]. In February 1996, EBO virus surfaced again in Makokou, Gabon, claiming 21 lives (56.8% mortality) [25, 26]. Clearly, EBO virus has reemerged as a serious public health concern. This concern has intensified due to the lack of filovirus vaccines and effective treatment regimens and because of the potential for widespread dissemination.

Little is known about the pathogenesis of filovirus infections. Previous studies of natural human outbreaks or of experimentally infected primates have described the clinical signs, histopathologic lesions, hematologic shifts, coagulopathies, and antigen distribution of filoviral disease [4–11]. However, with few exceptions, these investigations examined monkeys killed when moribund or those succumbing to infection and shed little light on the pathogenesis of EBO infection before death.

To investigate the early pathogenic events of EBO-Z infection, we examined tissues from EBO-infected guinea pigs killed at serial time points during the course of infection. We sought to identify those cells and tissues initially infected by EBO virus and thereby aid in defining the early targets for potential treatments.

Experiments done in our laboratory and by others [27–30] indicated that guinea pigs were susceptible to infection by filoviruses, and there is precedence for using guinea pigs as animal models to study viral hemorrhagic fevers. Guinea pigs have been used successfully as a model for human viral hemorrhagic fevers caused by several arenaviruses (Lassa fever virus, Junin virus, and Guanarito virus) [31–33]. The studies showed that there are quantitative and qualitative similarities among the disease processes of these viruses in guinea pigs, nonhuman primates, and humans. We undertook this study to compare

In conducting research using animals, the investigators followed the ''Guide for the Care and Use of Laboratory Animals,'' prepared by the Committee on Care and Use of Laboratory Animals of the Institute of Laboratory Animal Resources, National Research Council (National Institutes of Health Publication No. 86-23, revised 1985). The facilities are fully accredited by the American Association for Accreditation of Laboratory Animal Care.

The views, opinions, and findings contained herein are those of the authors and should not be construed as an official Department of the Army position, policy, or decision unless designated by other documentation.

This work was performed while Dr. Connolly held a National Research Council–USAMRIID research associateship.

Reprints or correspondence: Dr. Peter B. Jahrling, Headquarters, USAMRIID, Fort Detrick, Frederick, MD 21702-5011 (PBJ@DETRICK.ARMY.MIL).

The Journal of Infectious Diseases 1999; 179(Suppl 1):S203–17

0022–1899

EBO virus infection in guinea pigs with that in the primate models and to use the guinea pig model to explore the pathogenesis of EBO hemorrhagic disease.

Materials and Methods

Virus adaptation. All manipulations of EBO virus stocks, guinea pigs, and unfixed tissues or blood were conducted within a maximum-containment laboratory (biosafety level 4) at the United States Army Medical Research Institute of Infectious Diseases (USAMRIID). EBO-Z (Mayinga strain of EBO virus) was obtained as the original human serum specimen (057931) and passed once in Vero cell cultures. To achieve uniform lethality, the supernatants were titrated, adjusted to $10^{3.8}$ pfu EBO/0.2 mL, and inoculated subcutaneously (sc) over the back into 7 strain 13 guinea pigs. Seven days after inoculation, 2 guinea pigs were killed, and their spleens were removed, homogenized, titrated, and diluted to contain $10^{3.8}$ pfu/0.2 mL to serve as inoculum for 7 more guinea pigs. This process was repeated until uniform lethality was achieved at passage four.

Inoculation of guinea pigs. Inbred strain 13 guinea pigs (15 male, 15 female) were obtained from the USAMRIID colony. The guinea pigs were weighed, housed in groups of 3 to 4, and provided commercial guinea pig chow and fresh water ad libitum. Twenty-six guinea pigs were inoculated sc in the right upper thoracic limb with the guinea pig–adapted EBO (Mayinga strain) virus ($10^{3.8}$ pfu/0.5 mL PBS). The remaining 4 guinea pigs served as sham-inoculated controls and received 0.5 mL of PBS.

Necropsy. Groups of 4 EBO-infected guinea pigs were weighed, killed, and necropsied on each of postinoculation (pi) days 1–5. Groups of 3 EBO-infected guinea pigs were necropsied on pi days 7 and 9, and 1 control guinea pig was necropsied on each of pi days 1, 3, 5, and 9.

Before the guinea pigs were killed, whole blood was obtained by cardiac puncture for hematology counts, serum biochemical assays, and infectious virus titration. Portions of liver, spleen, pancreas, kidney, adrenal, and lung were removed aseptically and frozen at −70°C for virus infectivity assays. Additional portions of liver, lung, spleen, adrenal, and axillary lymph nodes were immersion-fixed in 4% paraformaldehyde plus 1% glutaraldehyde in 0.1 mol/L Millonig's phosphate buffer (pH 7.4) and processed for ultrastructural examination.

The following tissues were collected and immersion-fixed in 10% neutral-buffered formalin for histopathology, immunohistochemistry, and in situ hybridization: liver, spleen, lung, adrenal, kidney, pancreas, thyroid, thymus, esophagus, trachea, heart, stomach, small intestine, cecum, colon, urinary bladder, submandibular salivary gland, brain, skull, tongue, tonsil, uterus, testes or ovary, right and left axillary lymph nodes, mandibular lymph nodes, and mesenteric lymph nodes. In some animals, inguinal lymph nodes were also collected on pi days 4–9.

Histology and electron microscopy. Formalin-fixed tissues were routinely processed, embedded in paraffin, sectioned at 4–6 μm, and stained with hematoxylin and eosin for histopathology (bone samples were decalcified in 10% EDTA, pH 6.95, before processing). For electron microscopy studies, tissues were post-fixed in 1.0% osmium tetroxide in 0.1 *M* Millonig's phosphate buffer, rinsed, stained with 0.5% uranyl acetate, dehydrated in ethanol and propylene oxide, and embedded in resin (POLY/BED 812; Polysciences, Warrington, PA). Ultrathin sections were cut, placed on 200-mesh copper electron microscopy grids, stained with uranyl acetate and lead citrate, and examined with an electron microscope (JEOL 1200 EX; JEOL, Peabody, MA) at 80 KV.

Immunohistochemistry. Immunostaining for EBO viral antigens was performed by the labeled streptavidin-biotin method [34]. In brief, slides were digested with 0.05% protease VIII (Sigma Chemical, St. Louis) and incubated for 1 h with an anti-EBO mouse ascitic fluid that contained two monoclonal antibodies recognizing EBO virus glycoprotein and a filovirus matrix protein (VP40). Sections were then incubated with biotinylated horse anti-murine IgG (1:200; Vector Laboratories, Burlingame, CA) followed by alkaline phosphatase–conjugated streptavidin (Life Technologies Gibco BRL, Gaithersburg, MD). Bound antibody was detected with naphthol AS-BI phosphate–hexanized new fuchsin (Histomark Red; Kirkegaard & Perry, Gaithersburg), and sections were counterstained with Mayer's hematoxylin. Immunoreactive cells were identified by bright red cytoplasmic staining. In addition, selected sections were immunostained as above, except that peroxidase-conjugated streptavidin with 3,3′-diaminobenzidine tetrahydrochloride–$NiCl_2$ chromogen was used, as described [35].

Isotype-identical anti-Marburg mouse ascitic fluid and nonimmune mouse serum served as negative ascitic fluid controls. Specimens from animals parenterally inoculated with reference strains of EBO-Z served as positive tissue controls. Tissues from uninfected guinea pigs or those infected with the Musoke strain of Marburg virus (or both) served as negative tissue controls.

In situ hybridization. Replicate 5-μm sections were floated on diethyl pyrocarbonate (DEPC; Sigma)–treated water, collected on glass slides (Superfrost/Plus; Fisher Scientific, Pittsburgh), and air dried. The sections were deparaffinized, rehydrated through graded alcohols to DEPC water, and treated with 2× standard saline citrate (SSC) and Tris-buffered saline (TBS; 50 m*M* Tris HCl, 0.15 *M* NaCl, 2 m*M* $MgCl_2$, pH 7.6) as previously described [36, 37]. Sections were placed in a humidified chamber and digested for 30 min at 37°C with 20 μg/mL nuclease-free proteinase K (Boehringer Mannheim, Indianapolis) in TBS. Slides were washed in DEPC water and then in PBS containing 0.2% glycine to stop protease activity.

Plasmid pCRII (Invitrogen, San Diego) containing a 2.03-kb EBO viral glycoprotein cDNA insert was provided by Kevin Gilligan (USAMRIID). Midi preparations and plasmid purifications were performed using the Jetstar 2.0 kit (Genomed, Research Triangle Park, NC) according to the manufacturer's instructions. The probe was labeled by nick translation with digoxigenin-11–dUTP (Boehringer Mannheim) according to the manufacturer's instructions and used without further modification.

The hybridization conditions were adapted, with modifications, from a previously outlined method [37]. The probe was denatured at 95°C for 5 min and placed on ice. Fifty microliters of hybridization solution (45% vol/vol deionized formamide [Ambion, Austin, TX], 4× SSC, 2 mg/mL bovine serum albumin [BSA], 25-ng digoxigenin-labeled probe, nuclease-free H_2O to 50 μL) was applied to precleaned (RNase Zap; Ambion) coverslips, which were placed on the tissue sections and incubated overnight at 37°C.

The slides were flooded with 1× SSC to remove coverslips. Sections were washed in 1× SSC and incubated for 15 min at room temperature in TBS containing 0.1% BSA and 0.1% Triton.

Table 1. Lethality and viremia concentrations in strain 13 guinea pigs inoculated with various passage levels of Ebola (Mayinga strain virus).

Guinea pig spleen passage	% dead (n = 10)	Geometric mean (SE)* viremia on day 7
0	20	
1	40	2.1 (0.7)
2	50	2.7 (1.7)
3	70	3.8 (1.2)
4	100	5.2 (0.3)

NOTE. Animals were inoculated subcutaneously with $10^{3.8}$ PFU of Ebola virus.

* Log_{10} pfu/mL plasma.

Sections were then covered with 300 μL of alkaline phosphatase–conjugated anti-digoxigenin antibody (Fab fragment; 1:600 in TBS–0.1% BSA; Boehringer Mannheim) for 45 min at 37°C. Sections were washed twice in TBS–0.1% BSA, rinsed in deionized water, and placed in chromogen buffer (100 m*M* Tris-HCl, 100 m*M* NaCl, 50 m*M* $MgCl_2$, pH 9.5). Bound antibody was demonstrated by incubating slides in nitroblue tetrazolium salt-5-bromo-4-chloro-3-indolyl phosphate (Sigma) for 1 h at 37°C. Slides were washed in water and counterstained with nuclear fast red (Vector Laboratories). Positive cells were identified by blue-purple cytoplasmic staining. Controls included use of an irrelevant probe (Venezuelan equine encephalitis virus), plasmid without the EBO glycoprotein insert, and uninfected tissue.

Hematology and serum chemistry. Total white blood cells, hemoglobin, hematocrit, and platelets were counted with a hematologic analyzer (model 890; Coulter Electronics, Hialeah, FL). Differential white blood cell counts were performed manually. Serum levels of alanine aminotransferase (ALT), aspartate aminotransferase (AST), alkaline phosphatase, blood urea nitrogen (BUN), creatinine, and lactic acid dehydrogenase (LDH) were measured by use of a chemical analyzer (model 250; Eastman Kodak, Rochester, NY).

Virus isolation. Infectious virus in plasma, liver, spleen, kidney, adrenal, lung, and pancreas was assayed by counting plaques on Vero E6 cells maintained as monolayers in 6-well plates under agarose, as previously described [15]. Tissue homogenates (10%) were prepared in Eagle MEM containing 10% fetal calf serum and clarified by centrifugation before being assayed.

Results

Virus Adaptation

Sequential sc passages (each adjusted to $10^{3.8}$ pfu) of EBO virus in strain 13 guinea pigs resulted in increased lethality with each passage level. In addition, there was a corresponding increase in viremia titers 7 days after inoculation (table 1). The mean day of death for guinea pigs inoculated with the adapted virus was 9.05 days (range, 8–11). Levels of viremia increased from undetectable titers on day 1 to 5.2 log_{10} pfu/mL on day 7. Peak viremia titers in guinea pigs inoculated with the adapted virus were ~10- to 30-fold less than peak viremia titers in monkeys infected with the parental Mayinga strain (figure 1). Likewise, virus titers in tissues of moribund guinea pigs were qualitatively similar but quantitatively less (1–2 log_{10} pfu/g) than virus titers in corresponding tissues from lethally infected monkeys [34] (figure 2). Guinea pigs exhibited few clinical signs until around day 7, when they ceased eating and became febrile and dehydrated. Death usually occurred around day 9 and was not accompanied by visible signs of hemorrhage.

Virus Titers in Blood and Tissues

Onset of plasma viremia was rapid, occurring within 48 h, and ranged from 1.4 to 2.2 log_{10} pfu/mL (mean, 1.8). Peak viremia (mean of 5.2 log_{10} pfu/mL) occurred on day 7. While virus was associated with peripheral blood leukocytes, this interaction was not quantitated. In tissues, infectious virus was first detected on day 2 in spleen and liver, suggesting these organs are early sites of viral replication, and on day 3 in kidney, adrenal, lung, and pancreas (table 2). Mean organ titers rose progressively and reached their highest levels (4.8–6.4 log_{10} pfu/g) on day 9. The highest titers were recorded in the spleen, followed by adrenal, lung, liver, pancreas, and kidney.

Gross findings. There was a progressive weight loss in the EBO-infected guinea pigs, as determined by comparing initial weights with necropsy weights: The mean weight was −2.0% on day 5, −11.3% on day 7, and −23.3% on day 9. Control animals did not experience weight loss.

Necropsies of the 26 EBO-infected guinea pigs revealed the following: The right axillary lymph nodes were enlarged and reddened on day 1 in 1 of 4 guinea pigs. By day 3 and continuing through day 9, right axillary lymph nodes of all infected guinea pigs were enlarged (1.5–4 times normal size). Lymphadenopathy of the left axillary lymph nodes first appeared on day 4 (4/4 guinea pigs) and was a consistent finding through day 9. Lymphadenopathy of mandibular (3/4 guinea pigs), mesenteric (2/4 guinea pigs), and inguinal (1/3 guinea pigs) nodes was observed by days 4, 4, and 7, respectively.

The liver exhibited a mottled reticulated pattern on the capsular surface at days 4 and 5 (2/8 guinea pigs). On days 7 and 9, the liver was diffusely pale and friable (6/6 guinea pigs). On day 7, the spleens were slightly enlarged (3/3 guinea pigs), and the contents of the small intestine and cecum were watery (2/3 guinea pigs). Additional findings included scattered cortical petechiae of the kidneys and gastric erosions in the distal fundus of the stomach (1/3 guinea pigs).

On day 9, adrenal glands were enlarged (2/3 guinea pigs), the apical portion of the uterine horns appeared hyperemic (2/2 females) and enlarged, and white Peyer's patches of the small intestine were easily identified (2/3 guinea pigs). The stomach was nearly devoid of ingesta (2/3 guinea pigs), with focal hemorrhage in 1 guinea pig, and the contents of the small intestine were watery (2/3 guinea pigs). Ingesta in the proximal colon appeared tinged with blood, and disseminated petechiae

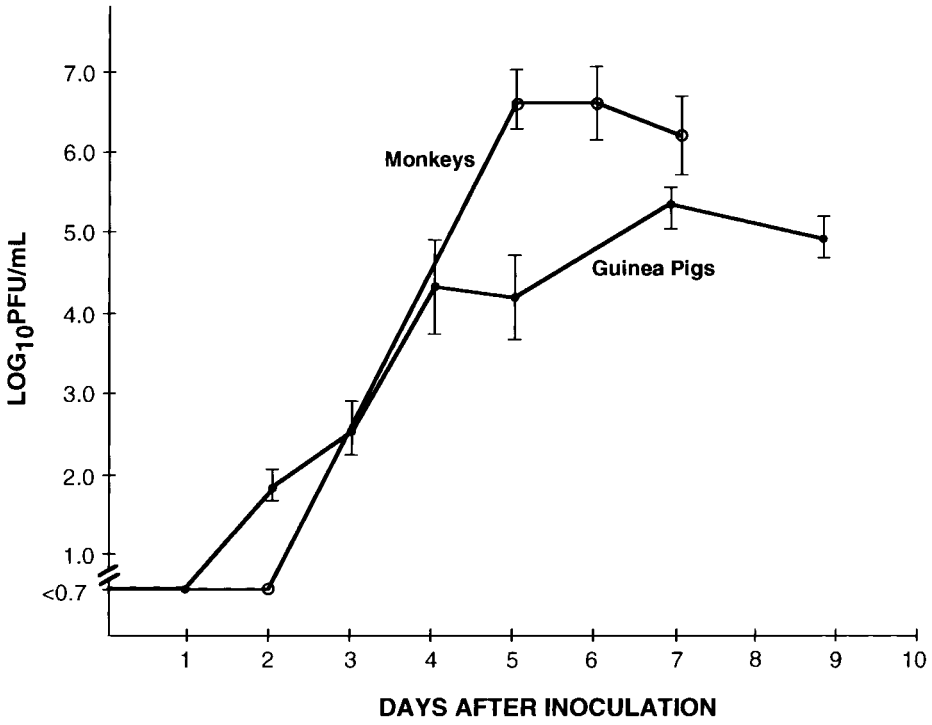

Figure 1. Comparison of plasma viremia titers in cynomolgus monkeys ($n = 6$) intramuscularly inoculated with EBO-Z (Mayinga strain, $10^{4.0}$ pfu) vs. strain 13 guinea pigs ($n = 8$) subcutaneously inoculated with guinea pig–adapted Ebola virus ($10^{3.8}$ pfu). Points are geometric mean ± SE.

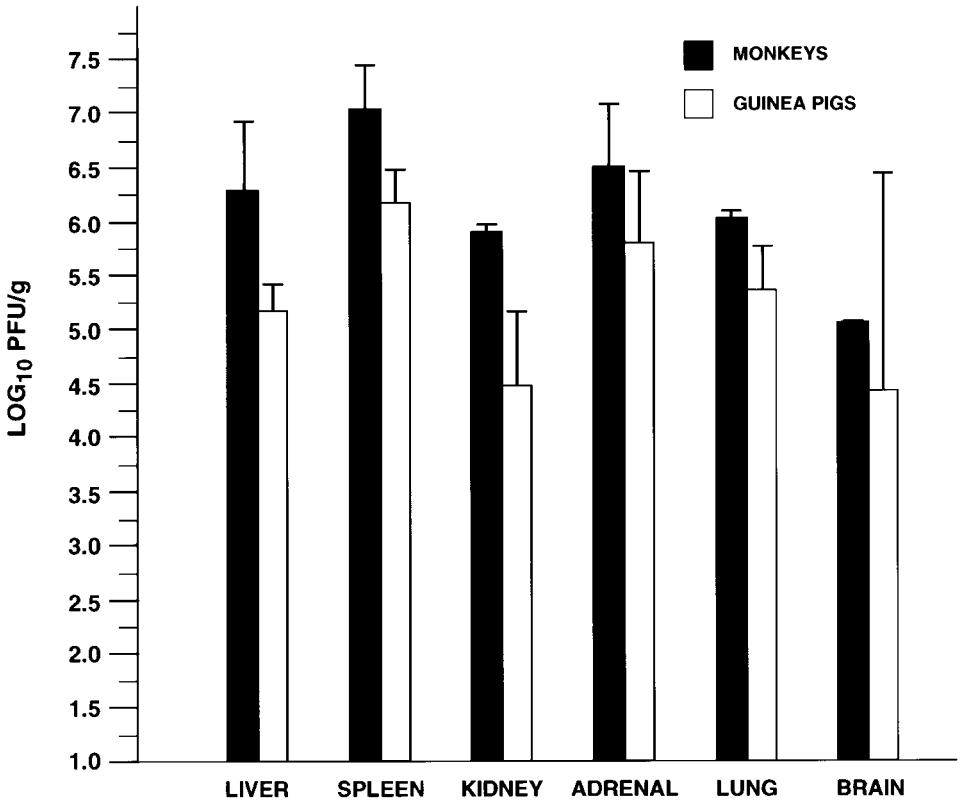

Figure 2. Comparison of infectivity titers in tissues of moribund cynomolgus monkeys intramuscularly inoculated with EBO-Z (Mayinga strain, $10^{4.0}$ pfu) vs. strain 13 guinea pigs subcutaneously inoculated with guinea pig–adapted Ebola virus ($10^{3.8}$ pfu). Points are geometric mean ± SE.

Table 2. Mean infectivity of guinea pig tissue homogenates (10% wt/vol) inoculated with EBO-Z (adapted Mayinga strain).

Postinoculation day	Geometric mean (SE) $\log_{10}$ pfu/mL or g						
	Plasma	Spleen	Liver	Adrenal	Lung	Kidney	Pancreas
1	<0.7 (0.0)	<1.7 (0.0)	<1.7 (0.0)	<1.7 (0.0)	<1.7 (0.0)	<1.7 (0.0)	<1.7 (0.0)
2	1.6 (.85)	2.6 (1.2)	1.8 (1.2)	<1.7 (0.0)	<1.7 (0.0)	<1.7 (0.0)	<1.7 (0.0)
3	2.5 (.88)	3.6 (.74)	2.5 (1.3)	1.3 (.95)	1.4 (1.2)	1.2 (.80)	1.2 (.80)
4	4.3 (1.3)	5.7 (.71)	4.5 (1.5)	3.6 (1.7)	3.9 (.86)	3.4 (1.4)	2.1 (2.5)
5	4.2 (1.4)	6.1 (.85)	5.0 (1.5)	3.7 (2.3)	3.1 (2.6)	3.3 (1.8)	<1.7 (0.0)
7	5.2 (.25)	6.3 (.53)	5.3 (.21)	6.2 (.55)	5.3 (.51)	4.8 (.86)	3.9 (1.7)
9	5.0 (.21)	6.4 (.21)	5.5 (.49)	6.0 (.92)	5.6 (0.0)	4.8 (.71)	5.8 (.85)

NOTE. Animals were inoculated subcutaneously with $10^{3.8}$ pfu of EBO-Z.

were present on the lungs (1/3 guinea pigs). Necropsies of the 4 control guinea pigs were unremarkable.

Hematology and clinical chemistry. Total and differential white blood cell counts revealed developing leukocytosis due to an increasing neutrophilia (table 3). By day 3, the mean white blood cell counts were twice baseline values. Mean neutrophil counts ranged from 2.0×10^3 cells/mm^3 on day 1, to 7.5×10^3 cells/mm^3 on day 9 (a >3.5-fold increase). There was a concomitant absolute lymphopenia as mean lymphocyte counts declined from 7.5×10^3 cells/mm^3 on day 1 to 2.3×10^3

Table 3. Hematology and serum enzyme values of guinea pigs inoculated subcutaneously with EBO-Z (adapted Mayinga strain) virus.

Guinea pig no.	Postinoculation day	Sex	Viremia ($\log_{10}$ pfu/mL)	Platelets	WBC ($\times 10^3$/mm^3)	PMNL (%)	Lym (%)	Mono (%)	AST (IU/L)	ALT (IU/L)	LDH (IU/L)	Alk phos (IU/L)	BUN (mg/dL)	Serum crt (mg/dL)
C1-1	1	F	<0.7	478,000	4.9	18	76	6	37	53	117	198	15	0.5
C1-2	1	F	<0.7	419,000	2.6	21	71	8	58	47	184	358	12	0.4
C1-3	1	M	<0.7	399,000	2.9	24	72	4	93	62	422	261	13	0.5
C1-4	1	M	<0.7	319,000	3.8	18	81	1	47	53	130	250	17	0.5
C2-1	2	F	<0.7	421,000	5.8	23	74	3	35	41	213	209	15	0.4
C2-2	2	F	2.2	592,000	6.9	32	65	3	170	45	1213	256	17	0.4
C2-3	2	M	1.1	384,000	6.4	36	62	2	92	54	291	266	13	0.6
C2-4	2	M	2.2	463,000	6.9	33	62	5	88	58	287	210	16	0.5
C3-1	3	M	1.4	396,000	6.0	41	55	4	66	50	184	224	11	0.5
C3-2	3	M	2.8	468,000	5.9	33	65	2	223	67	881	276	18	0.5
C3-3	3	F	3.5	486,000	4.6	48	49	3	69	51	340	42	20	0.7
C3-4	3	M	2.4	450,000	7.9	41	57	2	789	70	1698	171	20	0.5
C4-1	4	F	6.2	359,000	10.6	51	43	6	431	53	1758	257	20	0.4
C4-2	4	M	3.9	359,000	5.1	36	61	3	82	54	280	241	14	0.6
C4-3	4	M	3.4	406,000	6.3	35	61	4	93	46	448	282	15	0.5
C4-4	4	F	3.6	538,000	7.4	37	59	4	58	34	106	136	22	0.8
C5-1	5	F	3.8	299,000	5.8	39	57	4	229	52	1168	211	21	0.8
C5-2	5	F	5.2	226,000	7.0	33	28	6	190	58	743	159	15	0.6
C5-3	5	M	2.4	390,000	13.2	46	52	2	38	41	139	242	19	0.8
C5-4	5	M	5.3	221,000	6.6	68	27	5	125	56	413	226	16	0.7
C6-1	7	F	5.2	34,000	3.4	69	37	4	917	75	3795	340	49	0.7
C6-2	7	F	5.5	27,000	2.2	62	35	3	525	57	2547	282	23	0.7
C6-3	7	M	5.0	49,000	4.7	71	25	4	525	81	1978	253	24	0.8
C7-1	9	F	5.1	109,000	10.7	68	29	3	1464	109	4532	813	172	2.3
C7-2	9	F	4.8	64,000	11.2	82	17	1	897	94	1922	768	153	1.9
Control	1	F	<0.7	626,000	4.9	18	80	2	62	59	156	256	14	0.5
Control	3	M	<0.7	455,000	5.0	21	78	1	307	65	257	215	12	0.5
Control	5	F	<0.7	534,000	4.9	26	73	1	156	45	643	232	13	0.4
Control	9	M	<0.7	498,000	6.6	4	44	52	105	47	495	244	15	0.3

NOTE. WBC = white blood cell count, PMNL = neutrophils, Lym = lymphocytes, Mono = monocytes, AST = aspartate aminotransferase, ALT = alanine aminotransferase; LDH = lactic acid dehydrogenase, Alk phos = alkaline phosphatase, BUN = blood urea nitrogen, Serum crt = serum creatinine.

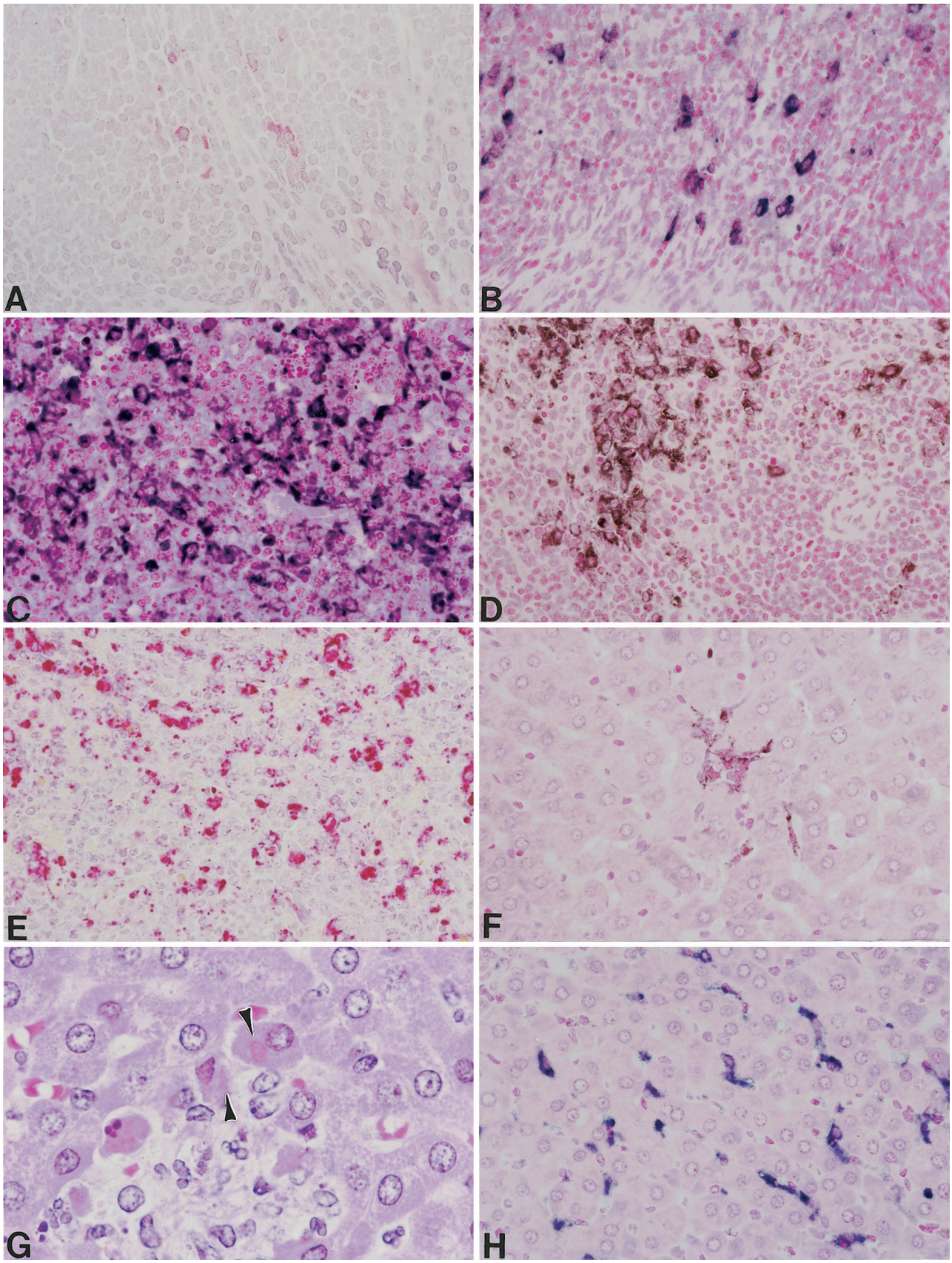

cells/mm^3 on day 9 (table 3). Thrombocytopenia developed as platelets declined precipitously from a preinfection mean of 533 $\times$ 10^3/mm^3 to 36.7 $\times$ 10^3/mm^3 on day 7 (table 3). Hemoglobin, hematocrit, and erythrocyte counts were unremarkable.

Early serum enzyme levels were unremarkable, but all were elevated during the late stage of disease (table 3). Elevations in LDH were striking after day 7 (range, 1922–4532 IU/L). On days 7 and 9, AST rose sharply, averaging 865 IU/L (range, 525–1464). However, there was only a modest (~2-fold) elevation of ALT during these later stages of disease. Alkaline phosphatase levels were terminally increased by almost 4-fold over baseline values. BUN levels remained generally within normal limits through day 7, after which, on day 9, there was a marked (10-fold over baseline) elevation. Serum creatinine levels increased on day 9.

Histology, Immunohistochemistry, In Situ Hybridization, and Ultrastructure

Lymph nodes. By immunohistochemistry, EBO viral antigen was detected within 24 h in a few (<10) macrophages in the right axillary lymph node in 2 of 4 guinea pigs (figure 3A); in situ hybridization revealed similar numbers of macrophages containing EBO virus RNA in all 4 guinea pigs. At 48 h, these axillary nodes exhibited a sizeable increase (~4- to 20-fold, compared with guinea pigs from day 1) in the number of macrophages containing viral antigen and RNA (figure 3B), and infection of macrophages was corroborated by electron microscopic demonstration of characteristic EBO intracytoplasmic virus nucleocapsid inclusions (figure 4) [39]. Thereafter, infection of right axillary node macrophages was consistent and progressive in all guinea pigs. At day 3, multifocal lymphoid necrosis in mesenteric lymph nodes and mild to moderate plasmacytosis in both the mediastinal and mandibular nodes was present in 1 guinea pig. Each of these lymph nodes contained antigen-positive cortical and sinus macrophages.

On day 4, macrophages in three of four left axillary nodes were antigen and RNA positive. In 1 animal, axillary, mesenteric, ileocecal, and mandibular lymph nodes were congested, there was necrosis of lymphocytes in the follicles, and many cortical and sinus macrophages contained viral antigen and RNA. Electron microscopy confirmed the light microscopy findings and identified occasional small deposits of fibrin in some lymphoid sinuses. Multifocal lymphoid necrosis and depletion of axillary, mandibular, mesenteric, ileocecal, and mediastinal lymph nodes was more consistent at day 5 (3/4 animals) and was diffuse on days 7 and 9. These nodes were enlarged by distention of the sinusoids with large histiocytic macrophages that contained abundant viral antigen. Numerous macrophages, sinus histiocytes, and sinus-lining cells were strongly positive for both viral antigen and RNA (figure 3C). Ultrastructurally, necrotic cellular debris, infected macrophages, free virions, and small clusters of fibrin were seen in the sinuses. By immunohistochemistry, in situ hybridization, or electron microscopy, we found no evidence of EBO infection of lymphocytes in any of the lymph nodes.

Spleen. Minimal, single-cell necrosis within the splenic red pulp was noted in 3 of 4 guinea pigs at day 2, with multifocal plasmacytosis in the lymphoid follicles in 1 animal. In 2 of 4 spleens, viral antigen was confined to occasional, scattered macrophages in the red pulp. At day 3, mild, multifocal necrosis extended beyond the red pulp to include the marginal zones and T cell–dependent periarteriolar sheaths (PALS). In 1 animal, there was moderate depletion of extramedullary hematopoietic cells. Antigen and RNA staining demonstrated scattered clusters and individual positive red pulp macrophages in all guinea pigs. Some macrophages contained eosinophilic, pleomorphic, intracytoplasmic inclusions. Few macrophages within the marginal zone were immunopositive, as were rare large, mononuclear, nonlymphoid cells within the white pulp.

On day 4, cellular depletion of hematopoietic elements in the red pulp and necrosis of the splenic white pulp, PALS, and red pulp were more extensive. Viral antigen and RNA were detected in red pulp macrophages and in antigen-presenting cells (i.e., dendritic and reticular cells) of some white pulp follicles (figure 3D). Electron microscopy revealed numerous circulating monocytes and tissue macrophages containing intracytoplasmic EBO virus inclusion material. Some virus-infected macrophages showed budding virions and clusters of virions along their plasma membranes. Free virions intermixed with cellular debris were seen in the red pulp, in marginal zones, and occasionally in blood vessels. Focally, small deposits of fibrin were present in the red pulp, usually in areas of degenerative macrophages.

Lymphoid necrosis and depletion in the splenic PALS involved ~25%–35% of the white pulp at day 5, and 2 guinea pigs developed antigen-positive histiocytic nodules in the red pulp. Red pulp macrophages continued to harbor viral antigen and RNA. By

Figure 3. Immunohistochemical (IHC) and in situ hybridization (ISH) demonstration of Ebola (EBO) viral antigen and viral RNA in strain 13 guinea pig lymph nodes, spleen, and liver. **A**, Right axillary lymph node. EBO viral antigen in macrophages 24 h after inoculation (IHC, alkaline phosphatase). **B**, Right axillary lymph node. EBO viral RNA in macrophages 48 h after inoculation (ISH). **C**, Mesenteric lymph node (postinoculation [pi] day 5). EBO viral antigen strongly positive in numerous macrophages (ISH). **D**, Spleen (pi day 4). EBO viral RNA in red pulp macrophages and in some antigen-presenting cells in white pulp (IHC; immunoperoxidase). **E**, Spleen (pi day 9). Abundant EBO viral antigen in red pulp macrophages (IHC; alkaline phosphatase). **F**, Liver (pi day 3). EBO viral antigen detected in necrotic foci and Kupffer's cells (IHC; immunoperoxidase). **G**, Liver (pi day 4). Intracytoplasmic viral inclusions (arrowheads) in hepatocytes surrounding necrotic focus (hematoxylin and eosin). **H**, Liver (pi day 5). EBO viral RNA staining is predominantly in the sinusoids (ISH). Original magnification: **A**, ×600; **B**–**F** and **H**, ×400; **G**, ×1000.

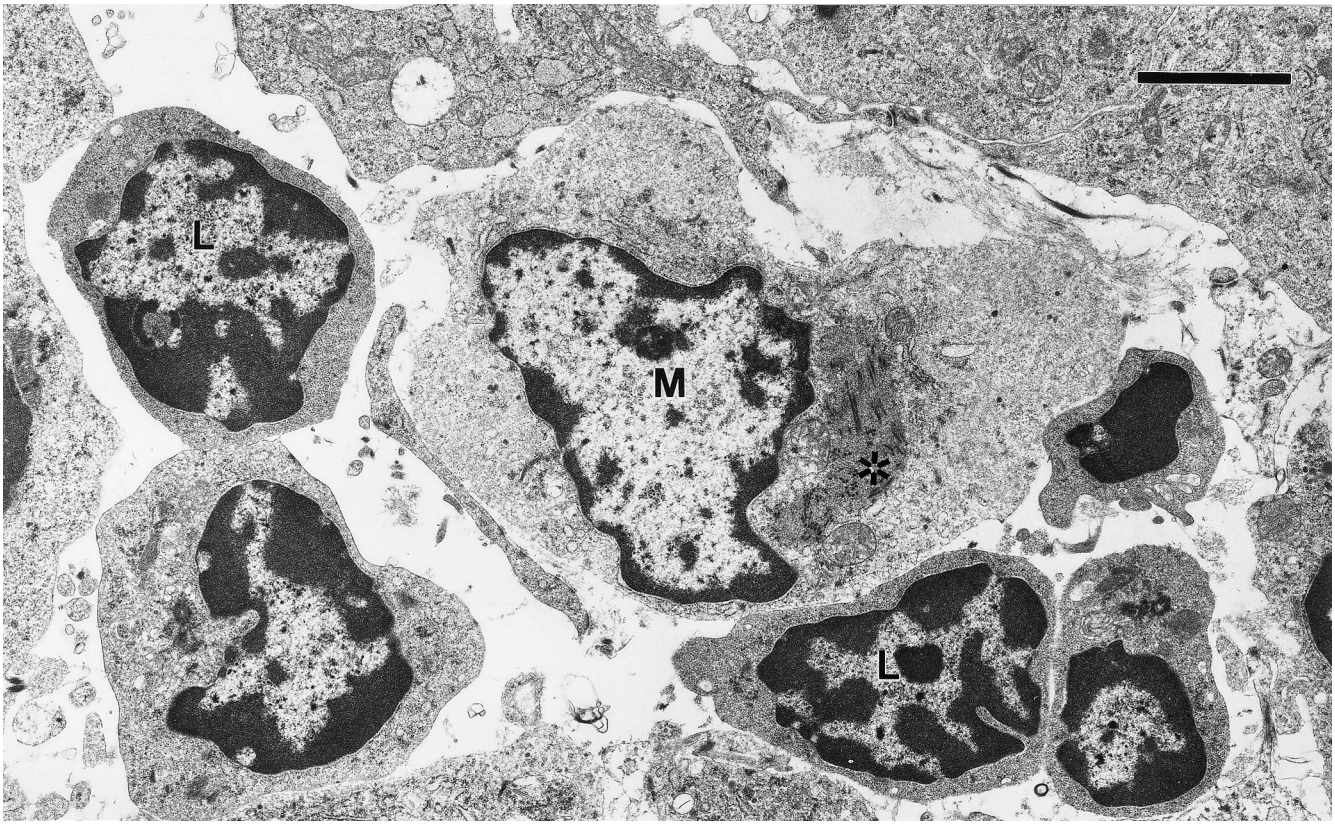

Figure 4. Electron micrograph of right axillary lymph node (postinoculation day 2). Ebola virus inclusion (*) in cytoplasm of a sinus macrophage (M). Lymphocytes (L) appear normal. Bar = 2.5 μm.

electron microscopy, modest amounts of fibrin and free virions were seen in the red pulp venous sinuses (figure 5). Lymphoid depletion and necrosis of the splenic follicles was accompanied by diffuse necrosis and congestion in the red pulp at days 7 and 9. Viral antigen and RNA staining persisted in macrophages and antigen-presenting cells (figure 3E). Ultrastructurally, the red pulp and marginal zones contained large fibrin deposits, numerous free virions, and virions enmeshed in fibrinocellular debris.

Liver. There were multiple, random, small foci of hepatocellular necrosis with a mild lymphocytic or neutrophilic infiltrate in 2 of 4 guinea pigs on day 2 and in 4 of 4 guinea pigs on day 3. On day 3, antigen-positive hepatocytes and Kupffer's cells were seen (figure 3F). On day 4, intracytoplasmic inclusions similar to the inclusions in splenic macrophages were seen within the hepatocytes surrounding the necrotic foci (figure 3G) and in Kupffer's cells. EBO antigen and RNA were detected in most of these foci and in numerous Kupffer's cells and circulating mononuclear cells. Sinusoids were dilated with antigen-positive cellular debris. By electron microscopy, free virions were observed in Disse's spaces, and EBO virus inclusions were seen in Kupffer's cells. At day 5, disseminated foci of hepatocellular necrosis in the livers of all guinea pigs were strongly immunoreactive; however, viral staining predominated in Kupffer's cells and sinusoids (figure 3H).

Examination (using an electron microscope) revealed that many degenerate and necrotic Kupffer's cells and some hepatocytes contained viral nucleocapsid inclusions. Free virions were observed in association with Kupffer's cell debris and in foci of hepatocellular necrosis. Sinusoids and Disse's spaces were expanded, and there was focal disruption of sinusoidal endothelium in areas where EBO virus was present. In some fields, small amounts of fibrin deposition were seen in the sinusoids. At day 7, hepatocellular vacuolar change and focal mineralization in areas of necrosis were seen in all EBO-infected guinea pigs. In addition to Kupffer's cells and foci of hepatocellular necrosis, fibroblast-like cells surrounding some portal triads contained viral antigen and RNA. At day 9, fibrin deposition was also more prevalent in the sinusoids and in the subendothelial spaces of the liver where it was intermixed with virions and cellular debris. EBO virus was frequently seen in subepithelial connective tissue of the bile ducts as free virions and as intracytoplasmic viral inclusions in degenerate fibroblasts.

Gastrointestinal Tract

Numerous immunopositive macrophages were first detected in the lamina propria and gut-associated lymphoid tissue (GALT) in the cecum and colon of 1 guinea pig on day 4;

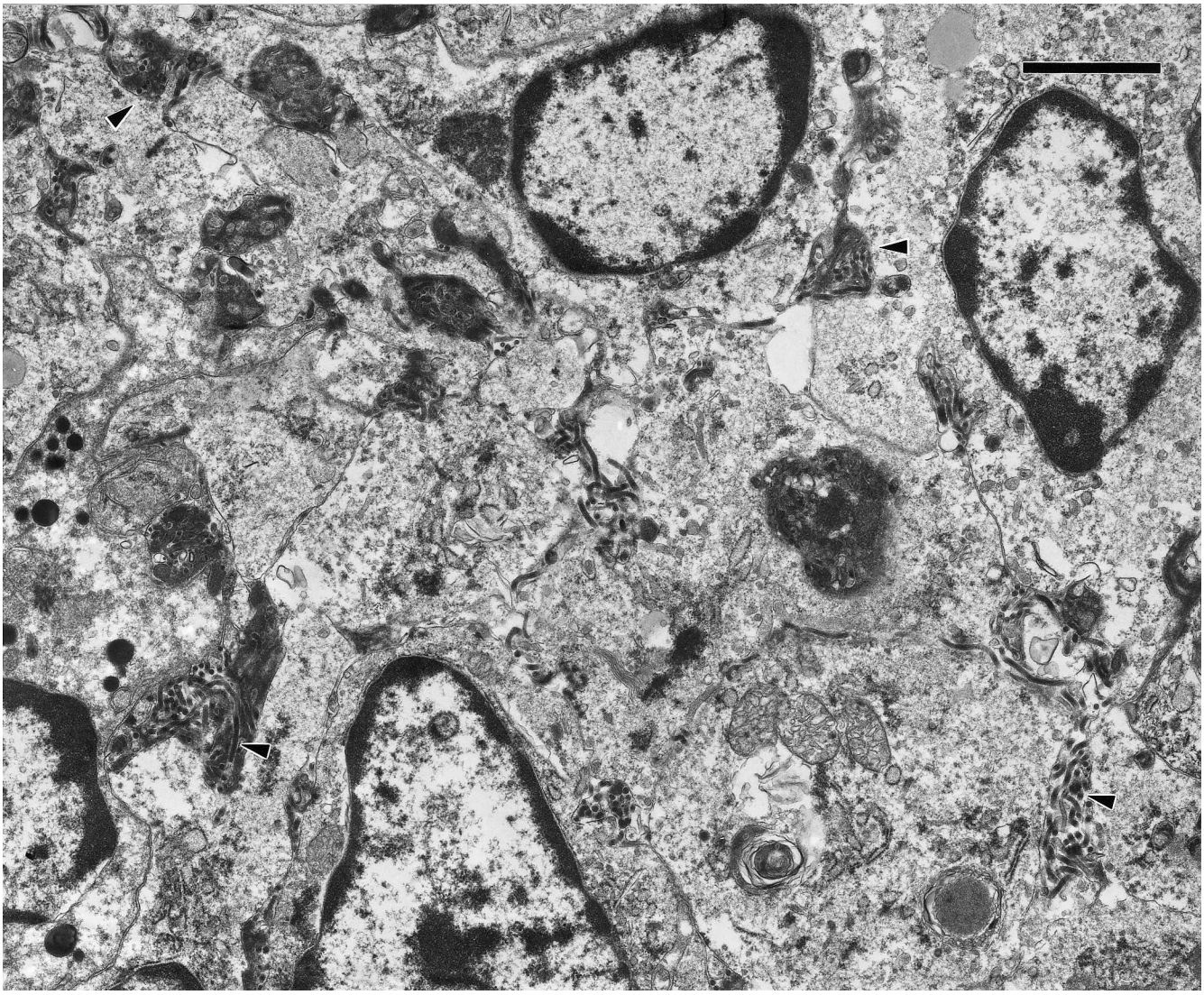

Figure 5. Electron micrograph of splenic red pulp (postinoculation day 5). Ebola virus particles (arrowheads) are present among small deposits of fibrinocellular debris between macrophages. Bar = 1.8 μm.

however, only rare immunopositive cells were noted within several foci of necrosis in the lamina propria of the stomach and small intestine. In 2 guinea pigs on day 5, viral antigen and RNA were seen in macrophages within the GALT and lamina propria (figure 6A) and in fibroblasts and macrophages surrounding intestinal glands.

On days 7 and 9, the consistent abundance of EBO viral antigen and RNA in the digestive tract was striking and not restricted to foci of necrosis. In the stomach, interstitial cells surrounding gastric glands were focally positive for viral RNA. Frequently, in the villar lamina propria of the small intestine, submucosa, and GALT, macrophages contained abundant EBO antigen and RNA. There was diffuse, marked necrosis in the lamina propria of the colon characterized by abundant karyorrhectic debris intermixed with antigen- and RNA-positive macrophages (figure 6B). Numerous interstitial macrophages and fibroblasts surrounding the intestinal crypts also contained viral RNA, as did fibroblasts throughout the submucosa. In some segments of the colon, viral RNA was detected in fibroblast-like cells within the circular layer of the muscularis externa.

Adrenal Gland

No significant adrenal lesions were present at day 4; however, in 1 guinea pig, viral antigen and RNA were detected in all three cortical zones. The most abundant staining was in the zona fasciculata, where EBO virus inclusions were ultrastructurally identified in some cortical cells, and free virions were seen in the adjacent subendothelial space. At day 5, viral antigen and RNA were observed in the adrenal cortex, primarily

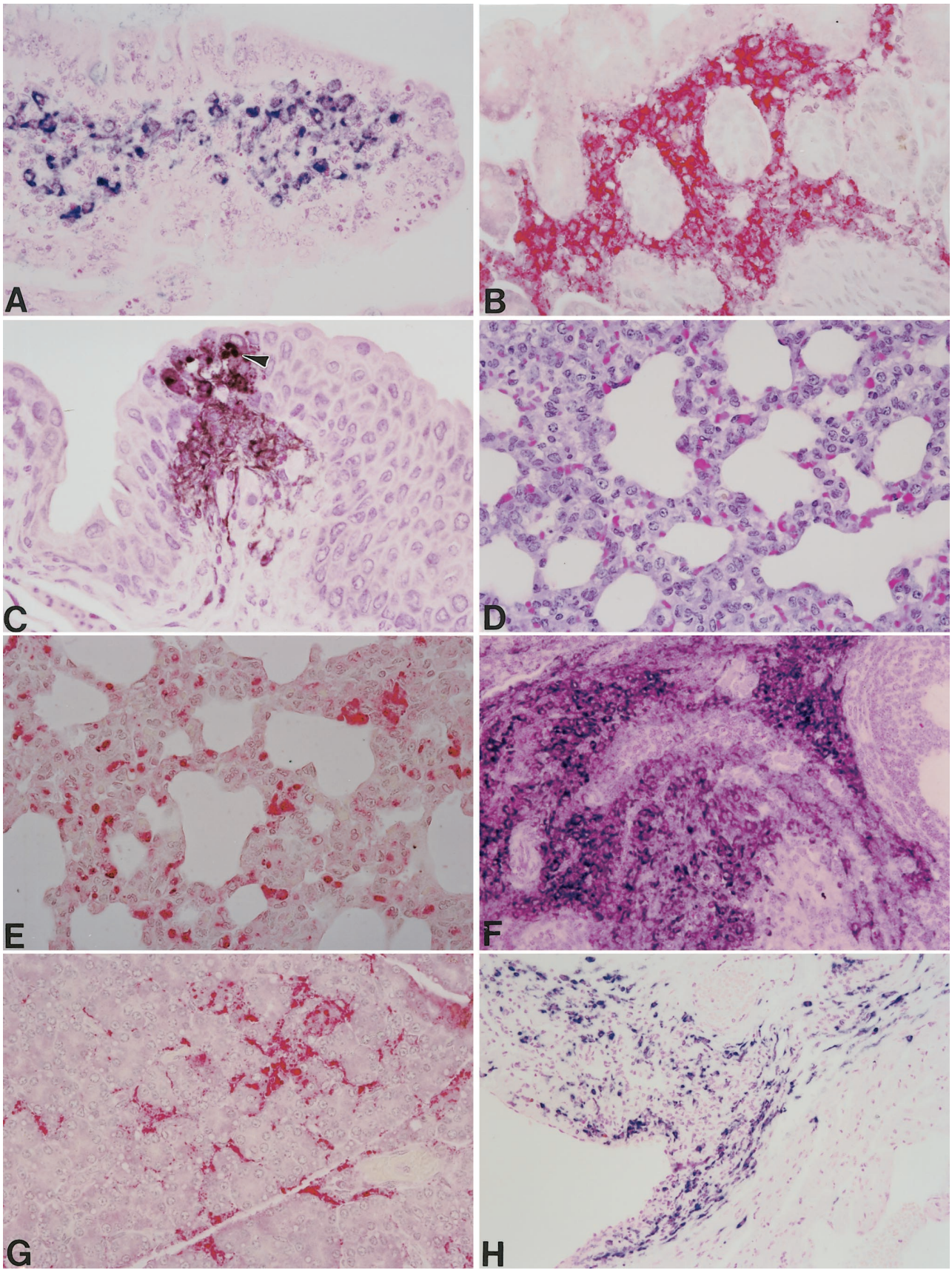

bordering sinusoidal capillaries, and in sporadic necrotic foci of the zona fasciculata. Small deposits of fibrin were sometimes seen in the cortical sinusoids. Adrenal gland infection was more extensive at days 7 and 9 and included multifocal localization of EBO viral antigen and RNA in the scattered necrotic foci of the zona fasciculata and zona reticularis.

Ultrastructurally at day 7, free virions and virions associated with cellular debris were frequently seen in the subendothelial spaces, particularly in areas adjacent to infected cortical cells and subendothelial fibroblasts. In the cortical sinusoids, endothelial cells were disrupted in areas where EBO virus was evident, and extravasated erythrocytes were seen in the subendothelial space. Only rarely were viral inclusions observed in sinusoidal endothelial cells. On day 9, the sinusoids were congested, and characteristic filovirus intracytoplasmic inclusions were seen in cortical cells of the zona fasciculata. Endothelial cell necrosis, occasional fibrin deposition, and free virions in cortical sinusoids were also observed by electron microscopy. Viral antigen was prevalent in foci of cortical necrosis, nonnecrotic cortical cells, interstitial cells subjacent to the sinusoids, and fibroblasts of the connective tissue capsule.

Kidney and Urinary Bladder

The kidneys were unremarkable until days 7 and 9, when scattered, peritubular cortical fibroblasts and macrophages contained viral antigen and RNA. In glomeruli, viral antigen and RNA appeared restricted to circulating monocytes in the capillaries. Electron microscopy examination confirmed these findings and identified infrequent fibrin deposits in intertubular blood vessels.

On days 4–9, the urinary bladder transitional epithelium was multifocally necrotic. The necrotic epithelial cells contained cytoplasmic viral inclusion bodies and were positive for viral antigen and RNA (figure 6C). At days 7 and 9, the submucosa of the bladder was edematous; viral infection of interstitial fibroblasts and macrophages was generally moderate, consisting of both individual and small foci of positive cells.

Lung

At days 1–5, there were mild perivascular lymphoid aggregates or granulomatous inflammation (or both) associated with inhalation (aspiration) of foreign material. In some animals on days 4 and 5, sporadic alveolar and interstitial macrophages were positive for viral antigen and RNA. Ultrastructurally, circulating monocytes containing EBO virus inclusions were infrequently seen in septal and interstitial pulmonary vessels, which also contained small amounts of fibrin. At days 7 and 9, multifocal to diffuse, lymphohistiocytic interstitial pneumonia was found in all EBO-infected guinea pigs (figure 6D). Viral antigen and RNA staining were consistently associated with thickened alveolar septa (figure 6E). Infected cells were primarily interstitial and alveolar macrophages, but there were also occasional foci of virus-infected fibroblasts in the peribronchial connective tissue. Some alveoli were congested with erythrocytes, leukocytes, pleural fluid, and fibrin. Viral infection also occurred occasionally in endothelial cells of pulmonary venules, and in subjacent fibroblasts and macrophages, where EBO virus inclusions and budding virions were evident (figure 7). Subepithelial foci of fibroblasts in the trachea were also multifocally positive for viral antigen and RNA.

Reproductive Organs

On day 4 in 1 of 2 females, there was focal immunoreactivity in ovarian thecal cells, despite the absence of any histologic lesions. In 2 of 2 females on day 7, abundant viral antigen and RNA were seen multifocally in ovarian and oviduct stromal cells and in theca follicular and theca lutein cells (figure 6F). Inflammation and necrosis of the uterine endometrial stroma and vascular tunic coincided with antigen-positive staining. In males after day 5, antigen-positive cells were seen in the interstitium of the testes.

Other Tissues

Viral infection in other tissues primarily involved connective tissue macrophages and fibroblasts and generally appeared at later time points (days 7 and 9) in the absence of histologic lesions. In the pancreas, EBO antigen and RNA were detected in scattered intralobular septal fibroblasts and macrophages at day 5 but became much more prevalent at days 7 and 9, when interlobular cells and small foci of acinar cells were also infected (figure 6G). Portions of peritoneal fat were remarkable for the ample amounts of viral RNA that were detected during the late stage of disease. Sections of thymus at day 7 revealed foci of large, positively stained mononuclear cells interpreted

Figure 6. Immunohistochemical (IHC) and in situ hybridization (ISH) demonstration of Ebola (EBO) viral antigen and viral RNA in strain 13 guinea pig tissues. **A**, Small intestine (postinoculation [pi] day 5). Viral RNA in macrophages and fibroblasts in villar lamina propria (ISH). **B**, Small intestine (pi day 9). Abundant viral antigen in macrophages and fibroblasts surrounding intestinal glands in colon (IHC; alkaline phosphatase). **C**, Urinary bladder (pi day 4). Viral antigen in submucosa and transitional epithelium. Note immunopositive intracytoplasmic inclusions (arrowhead) in epithelium (IHC; immunoperoxidase). **D**, Lung (pi day 7). Diffuse, lymphohistiocytic interstitial pneumonia (hematoxylin and eosin). **E**, Lung (pi day 7). Viral antigen in alveolar macrophages. (IHC; alkaline phosphatase). **F**, Ovary (pi day 7). Stromal cells contain copious amounts of EBO viral RNA (ISH). **G**, Pancreas (pi day 9). Viral antigen in intra- and interlobular fibroblasts and foci of acinar cells (IHC; alkaline phosphatase). **H**, Heart (pi day 9). EBO viral RNA in atrial myocardium (ISH). Original magnification: **A**–**E** and **G**, ×400; **F** and **H**, ×200.

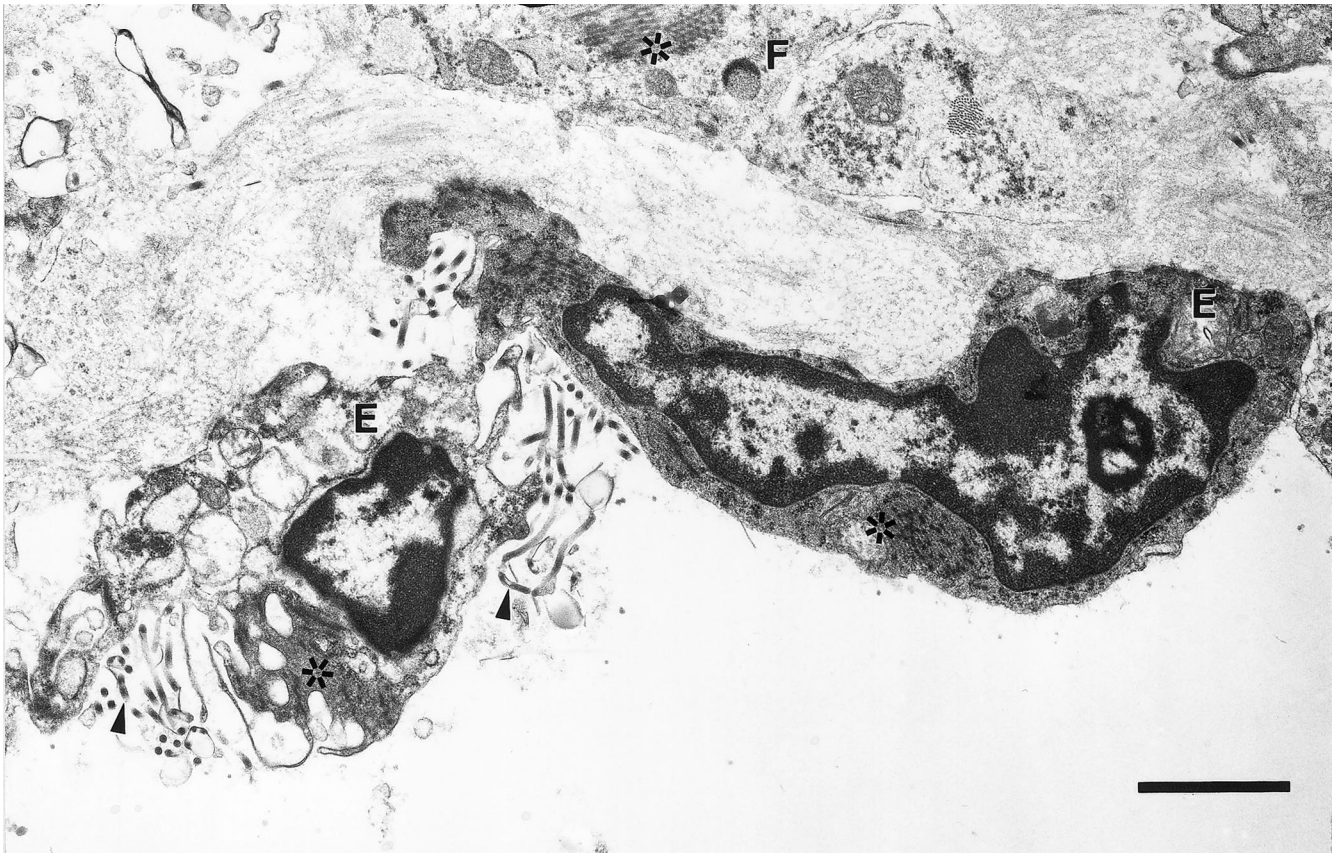

Figure 7. Electron micrograph of lung (postinoculation day 7). Ebola virus inclusions (*) in endothelial cells (E) of interstitial venule and subendothelial fibroblast (F). Note Ebola virions (arrowheads) budding from the endothelial cell into lumen of venule. Bar = 1.5 μm.

as epithelial reticular cells. Interstitial connective tissue cells in the thyroid were focally immunopositive, as were fibroblasts and macrophages in the lamina propria of the tongue, olfactory mucosa, dental pulp, and gingival submucosa. Viral infection of histiocytic cells in the bone marrow was evident beginning on day 4 and increased in number thereafter.

Mild to moderate multifocal inflammation in the heart coincided with viral antigen and RNA distribution in the atrial myocardium at days 7 and 9 (figure 6H). Antigen- and RNA-positive interstitial cells were also dispersed throughout the subepicardial connective tissue and ventricular endomysium.

Discussion

Infection of guinea pigs with reference strains of EBO virus usually produces only a transient febrile illness [29]. Thus, adaption of virus stocks by serial passage in guinea pig tissues is necessary to increase their pathogenicity in guinea pigs [28, 30]. In this study, we sc inoculated guinea pigs with EBO-Z (Mayinga strain) virus adapted to produce lethal infection by four sequential passages in EBO-infected guinea pig spleens. Guinea pigs killed sequentially after inoculation with the adapted virus developed lesions similar to those reported in monkeys and humans infected with the reference Mayinga strain.

In primates, EBO virus replicates to high titers in the spleen, liver, adrenal gland, lung, and blood. In our guinea pigs, EBO virus also replicated to high titers in these organs, although the peak levels were quantitatively somewhat less ($\sim$1–2 $\log_{10}$ pfu/g). We found that at each time point, virus titers were highest in the spleen; this finding is consistent with previous reports of samples from EBO-infected nonhuman primates at or near death [40]. Viremia in guinea pigs developed within 48 h of inoculation and increased during the course of the disease, reaching a peak on day 7.

It is clear from studies of moribund monkeys that EBO virus has a predilection for macrophages and monocytes [34, 35]. Our results show that in guinea pigs, as in primates, the primary targets of EBO virus are also macrophages, monocytes, and other cells (Kupffer's cells and antigen-presenting cells) of the mononuclear phagocyte system. In fact, these cells are the initial viral targets; as early as 24 h after inoculation, immunohistochemical and in situ hybridization assays detected viral antigen and viral RNA in macrophages of the right axillary lymph nodes. Further confirmation came from examination of

axillary lymph nodes on pi day 2, when sufficient numbers of macrophages were infected to allow virus identification by electron microscopy. There was a consistent increase in the number of infected macrophages in all guinea pigs on subsequent days as the disease progressed and as macrophage infection became most prevalent in lymphoid tissues.

Importantly, lymphocytes were not infected by EBO virus. We were unable to identify viral involvement of lymphocytes ultrastructurally or immunohistochemically or by detection of viral RNA, despite an ever-increasing lymphoid necrosis. In addition, attempts to infect lymphocytes in vitro with the different strains of EBO virus have been unsuccessful (Jahrling PB, unpublished data). The diffuse lymphoid depletion, necrosis, and congestion in the spleens and lymph nodes of our guinea pigs is also a common feature of EBO infections in primates [5, 10, 34, 42]. The mechanism(s) governing lymphoid necrosis in EBO infections of both primates and guinea pigs remains unclear, but it is almost certainly related to the extensive infection of macrophages and the resulting changes that take place within the microenvironment of lymphoid tissues.

Cells of the mononuclear phagocyte system are essential for both initiation and regulation of the immune response. Their early infection by EBO virus may represent a most effective strategy for evasion of the host defense system. A lack of an effective cellular immune response to EBO virus infection was evident in our guinea pigs, as it is in humans and nonhuman primates. We speculate that viral interference of the complex signaling mechanisms, which are generated by macrophages, that are responsible for activation of cell-mediated immunity could hinder EBO antigen presentation and EBO antigen–specific recognition, or interference could suppress T cell activity through down-regulation of specific cytokines. Indeed, the recent discovery of a conserved immunosuppressive motif in the C-terminal region of filoviral glycoproteins lends some credence to this speculation [43, 44], and the role of secreted EBO virus glycoprotein in suppression of neutrophil activation has recently been reported [45]. Conversely, EBO virus initially replicates and thrives in mononuclear phagocytic cells before their eventual destruction, thus effectively eliminating them and their repertoire of immunologic stimulatory factors. Future investigations may be able to provide insight into the specific immunologic events that transpire during EBO virus infection.

Virus-induced changes in the livers of infected guinea pigs were also similar to those reported in rhesus macaques and humans, including Kupffer's cell infection and multifocal necrosis of hepatocytes [5, 10, 34, 46]. In guinea pig livers, the initial and principal cell type infected was the Kupffer's cell. Foci of necrosis and infection of hepatocytes containing characteristic pleomorphic intracytoplasmic viral inclusions became more numerous on days 4–9, but these lesions were not sufficient to indicate organ failure. Furthermore, inflammatory cell infiltrates in the livers and other organs were generally mild, given the degree of necrosis and the large amounts of virus present.

Viral infection of portions of the gastrointestinal tract (particularly the cecum and colon) began at day 5, when macrophages and interstitial cells within the lamina propria were positive for viral antigen and RNA. Infection and necrosis of the lamina propria in the gastrointestinal tract (including portions of the small intestine) and GALT became widespread and severe on subsequent days. EBO virus infection of other guinea pig tissues (i.e., spleen, adrenal, lung, and ovary) became evident at days 4 and 5 and expanded within these tissues at later time points. In addition, as guinea pigs became moribund (days 7 and 9), there was widespread virus infection of the connective tissue interstitial cells (fibroblasts and fibrocytes) in many organs. Similar lesions and virus distributions have been reported in moribund primates [5, 34].

EBO virus infection causes aberrations in certain hematologic parameters [11, 42, 45–46]. For example, in moribund primates, leukocytosis as a result of marked neutrophilia is a fairly consistent finding, and frequently, there is a concomitant absolute lymphopenia. Neutrophilia and lymphopenia in our infected guinea pigs was detectable as early as day 2 and increased in severity over the course of ensuing infection. In humans, thrombocytopenia typically develops in acutely ill patients experiencing hemorrhagic symptoms, and loss of platelet function has been reported in experimentally infected primates [46, 47]. Although we did not measure platelet function, thrombocytopenia was marked during the later stages of disease when guinea pigs became moribund and platelets fell from a mean of 500,000 to $<$50,000/μL.

Fibrin deposition and endothelial cell involvement resulting from EBO (Mayinga strain) infection in moribund monkeys are variable. The magnitude of either of these events differs among primate species and among individual animals. In guinea pigs, direct infection of endothelial cells, although somewhat infrequent in the samples we examined, appeared first at day 7 in sections of lung and adrenal glands. Damage to the endothelium was also noted in portions of liver and adrenal during the later stages of infection in areas where adjacent cells but not endothelial cells were infected, suggesting that other mediators (e.g., tumor necrosis factor-α) may be responsible [48]. Similarly, fibrin deposition was a late event in the guinea pigs, beginning only modestly on day 4 (small amounts in the liver and spleen), with increases in distribution and amount on days 7 and 9, coincident with decreases in platelet counts. Others have shown that in EBO-infected guinea pigs, the degree of both endothelial cell infection, fibrin deposition, and vascular congestion increases with additional passage of the virus [29, 30]. Therefore, increasing the number of passages of the virus may be desirable in future guinea pig studies designed to study EBO-induced coagulopathies.

Abnormalities in other laboratory measurements, although by no means pathognomonic for filovirus infection, appear consistently in EBO infection of humans and other primates. Elevated levels of serum transaminases, LDH, and alkaline phosphatase occur during the later stages of EBO infection,

and terminal increases in BUN and serum creatinine have also been reported [42]. To some extent in humans, liver damage may be inferred from the marked elevations in AST seen in filovirus infections. However, the lesions are not so severe histologically as to suggest liver failure. Moreover, ALT levels (a more specific marker for liver damage in humans) are only modestly elevated. Our data show the same transaminase relationship held true in guinea pigs, in which both transaminase levels were increased, and there were high AST:ALT ratios. However, serum ALT and AST in guinea pigs and nonhuman primates (in contrast to humans) is not a specific indicator of hepatic disease, and other sources, such as cardiac or skeletal muscle, must be considered [49, 50].

Alkaline phosphatase and LDH were also increased in EBO-infected guinea pigs. Again, extrahepatic sources likely contributed to these increases; however, without isoenzyme analysis, identification of these sources is not possible. The infection in the guinea pig intestine may have contributed to high levels of alkaline phosphatase, particularly on day 9, when intestinal necrosis was extensive. The striking terminal elevations we observed in BUN, with only mild increases of serum creatinine and the absence of significant kidney lesions, may be due to dehydration or decreases in fluid volume (prerenal azotemia/shock).

In summary, our data support the use of guinea pigs as an animal model for experimental EBO virus infection. Immunohistochemical staining, in situ hybridization assays, and electron microscopy enabled us to identify macrophages and other cells of the mononuclear phagocyte system as the earliest cellular targets of EBO virus. The adapted virus produces a disease in guinea pigs that is in many ways comparable to EBO infection (from human isolates) in several monkey species and in humans (although present human data are limited). The quantitative differences seen in the virus titers of target organs of guinea pigs versus monkeys may be reduced by additional passage of the virus in guinea pigs. Nevertheless, the availability of a small animal model for studying filovirus infection should prove invaluable for initial screening of experimental vaccines, antiviral drugs, and immunotherapy regimens.

Acknowledgments

We thank Denise Braun, Joan Geisbert, Lynda Miller, and Amnart Churukha for their expert technical assistance.

References

1. Martini GA. Marburg virus disease: clinical syndrome. In: Martini GA, Siegert R, eds. Marburg virus disease. New York City: Springer-Verlag, **1971**:1–9.
2. Murphy FA, Simpson DIH, Whitfield SG, Zlotnik I, Carter GB. Marburg virus infection in monkeys. Lab Invest **1971**;24:279–91.
3. Gear JSS, Casal GA, Gear AJ, et al. Outbreak of Marburg virus disease in Johannesburg. Br Med J **1975**;4:489–93.
4. Bowen ETW, Platt GS, Lloyd G, Baskerville A, Harris WJ, Vell EC. Viral haemorrhagic fever in southern Sudan and northern Zaire. Lancet **1977**; 1:571–3.
5. Baskerville A, Bowen ET, Platt GS, McArdell LB, Simpson DI. The pathology of experimental Ebola virus infection in monkeys. J Pathol **1978**;125:131–8.
6. World Health Organization. Ebola haemorrhagic fever in Zaire, 1976. Bull WHO **1978**;56:271–93.
7. World Health Organization. Ebola haemorrhagic fever in Sudan, 1976. Bull WHO **1978**;56:247–70.
8. Smith DH, Francis DP, Simpson DIH. African haemorrhagic fever in the Southern Sudan, 1976. The clinical manifestations. In: Pattyn SR, ed. Ebola virus hemorrhagic fever. Amsterdam: Elsevier/North Holland Biomedical Press, **1978**:21–6.
9. Dietrich M, Schumacher HH, Peters D, Knobloch J. Human pathology of Ebola virus infection in the Sudan. In: Pattyn SR, ed. Ebola virus hemorrhagic fever. New York City: Elsevier/North Holland Biomedical Press, **1978**:37–42.
10. Baskerville A, Fisher-Hoch SP, Neild GH, Dowsett AB. Ultrastructural pathology of experimental Ebola haemorrhagic fever virus infection. J Pathol **1985**;147:199–209.
11. Fisher-Hoch SP, Platt GS, Neild GH, et al. Pathophysiology of shock and hemorrhage in a fulminating viral infection (Ebola). J Infect Dis **1985**; 152:887–94.
12. McCormick JB, Bauer SP, Elliot LH, Webb PA, Johnson KM. Biologic differences between strains of Ebola virus from Zaire and Sudan. J Infect Dis **1983**;149:264–7.
13. Richman DD, Cleveland PH, McCormick JB, Johnson KM. Antigenic analysis of strains of Ebola virus: identification of two Ebola virus serotypes. J Infect Dis **1983**;149:268–71.
14. Cox NJ, McCormick JB, Johnson KM, Kiley MP. Evidence for two subtypes of Ebola virus based on oligonucleotide mapping of RNA. J Infect Dis **1983**;149:272–5.
15. Jahrling PB, Geisbert TW, Dalgard DW, et al. Preliminary report: isolation of Ebola virus from monkeys imported to USA. Lancet **1990**;335: 502–5.
16. World Health Organization. Ebola virus—update. Wkly Epidemiol Rec **1990**;65:43.
17. World Health Organization. Viral hemorrhagic fever in imported monkeys. Wkly Epidemiol Rec **1992**;67:142–3.
18. Hayes CG, Burans JP, Ksiazek TG. Outbreak of fatal illness among captive macaques in the Philippines caused by an Ebola-related filovirus. Am J Trop Med Hyg **1992**;46:664–71.
19. Centers for Disease Control and Prevention. Ebola-Reston virus infection among quarantined nonhuman primates—Texas, **1996**;45:314–6.
20. Centers for Disease Control and Prevention. Update: filovirus infections among persons with occupational exposure to nonhuman primates. MMWR **1990**;39:266–7.
21. Centers for Disease Control and Prevention. Update: filovirus infection in animal handlers. MMWR **1990**;39:221.
22. Le Guenno B, Formenty P, Wyers M, Gounon P, Walker F, Boesch C. Isolation and partial characterisation of a new strain of Ebola virus. Lancet **1995**;345:1271–4.
23. Centers for Disease Control and Prevention. Outbreak of Ebola viral hemorrhagic fever—Zaire, 1995. MMWR **1995**;44:381–2.
24. Centers for Disease Control and Prevention. Update: outbreak of Ebola viral hemorrhagic fever—Zaire, 1995. MMWR **1995**;44:399.
25. Choo V: Ebola fever outbreak confirmed in Gabon. Lancet **1996**;347:528.
26. World Health Organization. Outbreak of Ebola haemorrhagic fever in Gabon officially declared over. Wkly Epidemiol Rec **1996**;71:125–6.
27. Bowen ETW, Platt GS, Lloyd G, Raymond RT, Simpson DIH. A comparative study of strains of Ebola virus isolated from southern Sudan and northern Zaire in 1976. J Med Vir **1980**;6:129–38.
28. Pereboeva LA, Tkachev VK, Kolesnikova LV, Krendeleva L, Ryabchikova EI, Smolina MP. The ultrastructural changes in guinea pig organs

during the serial passage of the Ebola virus. Vopr Virusol **1993**;38:179–82.
29. Ryabchikova EI, Baranova SG, Tkachev VK, Grazhdantseva AA. The morphological changes in Ebola infection in guinea pigs. Vopr Virusol **1993**;38:176–9.
30. Ryabchikova E, Kolesnikova L. Smolina M, et al. Ebola virus infection in guinea pigs: presumable role of granulomatous inflammation in pathogenesis. Arch Virol **1996**;141:909–21.
31. Jahrling PB, Smith S, Hesse RA, Rhoderick JB. Pathogenesis of Lassa virus infection in guinea pigs. Infect Immun **1982**;37:771–8.
32. Kenyon RH, Condie RM, Jahrling PB, Peters CJ. Protection of guinea pigs against experimental Argentine hemorrhagic fever by purified human IgG: importance of elimination of infected cells. Microb Path **1990**;9:219–26.
33. Hall WC, Geisbert TW, Huggins JW, Jahrling PB. Experimental infection of guinea pigs with Venezuelan hemorrhagic fever virus (Guanarito): a model of human disease. Am J Trop Med Hyg **1996**;55:81–8.
34. Jaax NK, Davis KJ, Geisbert TW, et al. Lethal experimental infection of rhesus monkeys with Ebola-Zaire (Mayinga) virus by the oral and conjunctival route of exposure. Arch Pathol Lab Med **1996**;120:140–55.
35. Davis KJ, Anderson AO, Geisbert TW, et al. Pathology of experimental Ebola virus infection in African green monkeys. Involvement of fibroblastic reticular cells. **1997.** Arch Path Lab Med 121:805–19.
36. Connolly BM, Jenson AB, Peters CJ, Geyer SJ, Barth JF, McPherson RA. Pathogenesis of Pichinde virus in strain 13 guinea pigs: an immunocytochemical, virological and clinical chemistry study. Am J Trop Med Hyg **1993**;49:10–24.
37. Guelin M, Kejzlarova-Lepesant J, Lepesant JA. In situ hybridization: a routine method for parallel localization of DNA sequences and their transcripts in consecutive paraffin sections with the use of ^{3}H-labelled nick translated cloned DNA probes. Biol Cell **1985**;53:1–12.
38. Pringle JH, Primrose L, Kind CN, Talbot IC, Lauder I. In situ hybridization demonstration of poly-adenylated RNA sequences in formalin-fixed paraffin sections using a biotinylated oligonucleotide poly d(T) probe. J Pathol **1989**;158:279–86.
39. Jahrling PB, Geisbert TW, Dalgard DW, et al. Preliminary report: isolation of Ebola virus from monkeys imported to USA. Lancet **1990**;335:502–5.
40. Geisbert TW, Jahrling PR. Differentiation of filoviruses by electron microscopy. Virus Res **1995**;39:129–50.
41. Bowen ETW, Platt GS, Simpson DIH, McArdell LB, Raymond RT. Ebola haemorrhagic fever: experimental infection in monkeys. Trans Royal Soc Trop Med Hyg **1978**;72:188–91.
42. Johnson E, Jaax N, White J, Jahrling P. Lethal experimental infections of rhesus monkeys by aerosolized Ebola virus. Int J Exp Pathol **1995**;76:227–36.
43. Sanchez A, Kiley MP, Holoway BP, Auperin DD. Sequence analysis of Ebola virus genome; organisation, genetic elements, and comparison with the genome of Marburg virus. Virus Res **1993**;29:215–40.
44. Sanchez A, Trappier SG, Mahy BWJ, Peters CJ, Nichal ST. The virion glycoproteins of Ebola viruses are encoded in two reading frames and are expressed through transcriptional editing. Proc Natl Acad Sci USA **1996**;93:3602–7.
45. Yang Z, Delgado R, Xu l, Todd RF, Nabel EG, Sanchez A, Nabel GJ. Distinct cellular interactions of secreted and transmembrane Ebola virus glycoproteins. Science **1998**;279:1034–7.
46. Peters CJ, Sanchez A, Rollin PE, Ksiazek TG, Murphy FA. Filoviridae: Marburg and Ebola viruses. In: Fields BN, Knipe BM, Howley PM, eds. Fields virology. Philadelphia: Lippincott-Raven Publishers, **1996**:1191–76.
47. Fisher-Hoch SP, Brammer TL, Trappier SG, et al. Pathogenic potential of filoviruses: role of geographic origin of primate host and virus strain. J Infect Dis **1992**;166:753–63.
48. Feldmann H, Bugany H, Mahner F, Klenk HD, Drenckhahn D, Schnittler HJ. Filovirus-induced endothelial leakage triggered by infected monocytes/macrophages. J Virol **1996**;70:2208–14.
49. Clampitt RB, Hart RJ. The tissue activities of some diagnostic enzymes in ten mammalian species. J Comp Pathol **1978**;88:607–21.
50. Hoffmann WE, Kramer J, Main AR, Torres JL. Clinical enzymology. In: Loeb WF, Quimby FW. The clinical chemistry of laboratory animals. 1st ed. New York City: Pergamon Press, **1989**:237–78.